Chapter 4

The effects of spectral line blending on photo-absorption

In chapter 3 the variation of the source function with respect to space was considered but in general it is also dependent on frequency. This dependence arises from any phenomenon that causes the emission and absorption profiles to be shifted and/or distorted with respect to one another. For example, photon scattering can lead to distorted emission profiles in the case of partial frequency redistribution. The probability of absorption (i.e. the opacity) is greatest at line centre but since there may be a change in direction of propagation in the scattering process, Doppler shifts can lead to a diffusion of photons toward the line wings. Also if a plasma is exposed to a radiation field which arises from a region that is moving relative to it, the resultant emission profiles will be distorted and asymmetric.

Another contributer to frequency dependence is spectral line blending. When two spectral lines overlap in frequency space, photons from one line may be absorbed by the other. This leads to an enhancement or deficit in the emergent line intensities depending on the nature of the overlap. For instance, if one line is thick and the other thin, then the thin one will be attenuated due to absorption of its photons by the thick line. Such absorption, however, will enhance the upper level of the thick transition and thus result in a relative enhancement of the thick line emission. Hence, in this instance, blending thickens the thin line and thins the thick one. Line shapes are also

influenced by the fact that photo-absorption will no longer be symmetric about line centre (the term $\bar{I}_\nu \phi(\nu)$ is not symmetric about ν_0 when there is line blending).

Fig. 2.10a shows an example of line blending in an opacity modified multiplet. Blending influences both the emission and absorption and so if escape probability techniques are to be used then account must be taken of blending within the escape probability and absorption factor expressions.

In this chapter line blending is considered within the escape probability framework. Spatially resolved quantities are derived as in chapter 3 and are used to calculate optically thick population distributions and limb-brightening curves in order to assess the validity of the line-of-sight averaged escape probability in the case of blended spectral lines.

4.1 Blended escape probabilities

Blending influences the probability of escape in that it increases the number of potential absorbers. Consider the case of M lines blended together. The monochromatic transmission factor of a line in the blend is

$$T_\nu(s_1, s_2) = exp\left\{-\sum_n \tau_\nu^{(n)}(s_1, s_2)\right\} \tag{4.1}$$

where $\tau_\nu^{(n)}(s_1, s_2)$ is the optical depth at frequency ν between two points s_1 and s_2 of the n^{th} line in the blend, i.e.

$$\tau_0^{(n)}(s_1, s_2) = \int_{s_1}^{s_2} \kappa_0^{(n)}(s) ds \tag{4.2}$$

Thus the escape probability is no longer purely a function of the optical depth of one line. Rather, it is dependent on a set of M optical depths, $\{\tau_0^{(n)}\}$. If it is assumed that all the lines in the blend have the same width (a reasonable assumption they are all of the same ion) and define υ_{in} as

$$\upsilon_{in} = \frac{\nu_0^{(i)} - \nu_0^{(n)}}{\Delta\nu_D} \tag{4.3}$$

then the mean escape probability of a photon emitted in line i at a point s along some line-of-sight is

$$g^{(i)}[\{\tau_0^{(n)}\},\{\upsilon_{in}\}] = \frac{1}{\sqrt{\pi}}\int_{-\infty}^{\infty} e^{-u^2} exp\left\{-\sum_n \tau_0^{(n)}(s)e^{-(u+\upsilon_{in})^2}\right\} du \qquad (4.4)$$

From this the blended line-of-sight averaged escape probability (formerly $\bar{g}\{\tau_0\}$) follows immediately as

$$\bar{g}^{(i)}[\{\tau_0^{(n)}\},\{\upsilon_{in}\}] = \frac{1}{\sqrt{\pi}}\int_{-\infty}^{\infty} e^{-u^2}\left[\frac{1-exp\left\{-\sum_n \tau_0^{(n)}e^{-(u+\upsilon_{in})^2}\right\}}{\sum_n \tau_0^{(n)}e^{-(u+\upsilon_{in})^2}}\right] du \qquad (4.5)$$

Both $g^{(i)}[\{\tau_0^{(n)}\},\{\upsilon_{in}\}]$ and $\bar{g}^{(i)}[\{\tau_0^{(n)}\},\{\upsilon_{in}\}]$ are prescribed by a set of optical depths,

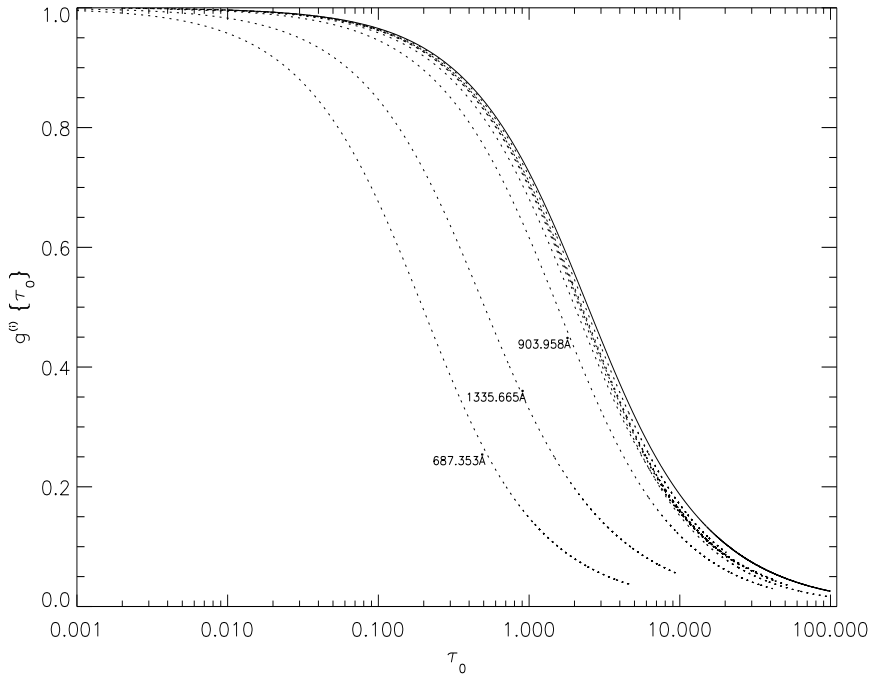

Figure 4.1: Line-of-sight averaged escape probabilities versus optical depth excluding line blending ($\bar{g}\{\tau_0\}$ – solid line) and including line blending for a selection of spectral lines of C II ($\bar{g}^{(i)}\{\tau_0\}$ – dotted lines). The three cases which deviate most markedly from the unblended result are labelled.

$\{\tau_0^{(n)}\}$ and a set of *overlap parameters* $\{\upsilon_{in}\}$. The latter are constants, though they

may act as variable parameters in an emission model or diagnostic. Furthermore, the set of optical depths may be related via eq. 2.24 and so the escape probabilities become prescribed by a single optical depth and a set of optical depth ratios, $\{\tau_0^{(n)}/\tau_0^i\}$. Thus $g^{(i)}[\{\tau_0^{(n)}\},\{\upsilon_{in}\}]$ and $\bar{g}^{(i)}[\{\tau_0^{(n)}\},\{\upsilon_{in}\}]$ become $g^{(i)}\{\tau_0\}$ and $\bar{g}^{(i)}\{\tau_0\}$ and may be plotted as functions of optical depth. Fig. 4.1 shows $\bar{g}^{(i)}\{\tau_0\}$ versus optical depth for a selection of C II spectral lines. It is evident from this graph that, as expected, the unblended result represents an upper limit since blending leads to additional attenuation due to overlapped components.

This does not negate the statement made above that blending can lead to an enhancement of a spectral line. Blending will always decrease the probability of escape but it will also lead to an enhancement of the upper levels of optically thick lines and thus to an enhancement in emission. The combined effect can be to enhance or deplete the emergent intensity. Which will be the case may be determined using a blended absorption factor.

4.2 The blended absorption factor

Photo-absorption at a point in a plasma is influenced by blending in two ways. Firstly, photons of more than one line may be absorbed. Secondly, those photons may be absorbed by a number of lines en-route. The blended absorption factor quantities may be derived following the same reasoning as before but with $j_\nu^{(tot)}$ and $\kappa_\nu^{(tot)}$ replacing j_ν and κ_ν where

$$j_\nu^{(tot)} = \sum_n j_\nu^{(n)} = \sum_n \frac{\omega_l^{(n)}}{\omega_u^{(n)}} \frac{2\nu_0^2}{c^2} \frac{N_u^{(n)}}{N_l^{(n)}} \kappa_\nu^{(n)} \tag{4.6}$$

with

$$\kappa_\nu^{(n)} = \kappa_0^{(n)} N_l^{(n)} e^{-(u+\upsilon_{in})^2} \tag{4.7}$$

$$\Rightarrow j_\nu^{(tot)} = \sum_n \frac{\omega_l^{(n)}}{\omega_u^{(n)}} \frac{2\nu_0^2}{c^2} N_u^{(n)} \kappa_0^{(n)} e^{-(u+\upsilon_{in})^2} \tag{4.8}$$

and

$$\kappa_\nu^{(tot)} = \sum_n \kappa_\nu^{(n)} = \sum_n \kappa_0^{(n)} N_l^{(n)} e^{-(u+\upsilon_{in})^2} \tag{4.9}$$

These give

$$\bar{\bar{g}}^{(i)}\{\tau_0/2\} = 1 - \frac{\omega_u^{(i)}}{\omega_l^{(i)}} \frac{N_l^{(i)}}{N_u^{(i)}} \int_{-\infty}^{\infty} \frac{c^2}{2\nu^2} \bar{I}_\nu \phi_\nu d\nu \tag{4.10}$$

with

$$\bar{I}_\nu = \frac{j_\nu^{(tot)}}{\kappa_\nu^{(tot)}} \left[1 - e^{-\kappa_\nu^{(tot)} x_1} + \kappa_\nu^{(tot)} x_1 E_1 \left\{\kappa_\nu^{(tot)} x_1\right\}\right] \tag{4.11}$$

Now

$$\begin{aligned} \frac{j_\nu^{(tot)}}{\kappa_\nu^{(tot)}} &= \frac{\sum_n \frac{\omega_l^{(n)}}{\omega_u^{(n)}} \frac{2\nu_0^2}{c^2} \frac{N_u^{(n)}}{N_l^{(n)}} \kappa_\nu^{(n)}}{\sum_n \kappa_0^{(n)} N_l^{(n)} e^{-(u+v_{in})^2}} \\ &= \frac{2\nu_0^2}{c^2} \frac{N_u^{(i)}}{N_l^{(i)}} \frac{\sum_n \frac{\omega_l^{(n)}}{\omega_u^{(n)}} \frac{N_u^{(n)}}{N_u^{(i)}} \frac{\kappa_0^{(n)}}{\kappa_0^{(i)}} e^{-(u+v_{in})^2}}{\sum_n \frac{\tau_0^{(n)}}{\tau_0^{(i)}} e^{-(u+v_{in})^2}} \end{aligned} \tag{4.12}$$

Therefore

$$\begin{aligned} \bar{\bar{g}}^{(i)}\{\tau_0/2\} = \; 1 - \; & \frac{\omega_u^{(i)}}{\omega_l^{(i)}} \frac{1}{\sqrt{\pi}} \int_{-\infty}^{\infty} e^{-u^2} \frac{\sum_n \frac{\omega_l^{(n)}}{\omega_u^{(n)}} \frac{N_u^{(n)}}{N_u^{(i)}} \frac{\kappa_0^{(n)}}{\kappa_0^{(i)}} e^{(u+v_{in})^2}}{\sum_n \frac{\tau_0^{(n)}}{\tau_0^{(i)}} e^{-(u+v_{in})^2}} \Bigg[1 - \\ & exp\left\{-\frac{1}{2} \sum_n \tau_0^{(n)} e^{-(u+v_{in})^2}\right\} + \\ & \frac{1}{2} \sum_n \tau_0^{(n)} e^{-(u+v_{in})^2} E_1 \left\{\frac{1}{2} \sum_n \tau_0^{(n)} e^{-(u+v_{in})^2}\right\}\Bigg] du \end{aligned} \tag{4.13}$$

$$\tag{4.14}$$

From this $\mathcal{G}^{(i)}(\tau_0, x)$ follows as

$$\mathcal{G}^{(i)}(\tau_0, x) = \frac{1}{2}\left(\bar{\bar{g}}^{(i)}\{\tau_0^+\} + \bar{\bar{g}}^{(i)}\{\tau_0^-\}\right) \tag{4.15}$$

Similarly

$$\Lambda^{(i)}(\tau_0, x_0) = 1 - \frac{\omega_u^{(i)}}{\omega_l^{(i)}} \frac{N_l^{(i)}(x_0)}{N_u^{(i)}(x_0)} \int \frac{c^2}{2\nu^2} \bar{I}_\nu \phi_\nu d\nu \tag{4.16}$$

with

$$\begin{aligned}\bar{I}_\nu &= \frac{1}{2}\left[\int_0^{x_0} j_\nu^{(tot)}(x)E_1\left\{\int_x^{x_0}\kappa_\nu^{(tot)}(x')dx'\right\}dx + \int_{x_0}^{\Delta x} \mathrm{J}_\nu^{(tot)}(x)E_1\left\{\int_{x_0}^{x}\kappa_\nu^{(tot)}(x')dx'\right\}\right] \\ &= \frac{2\nu_0^2}{c^2}\left[\int_0^{x_0}\sum_n \frac{\omega_l^{(n)}}{\omega_u^{(n)}}N_u^{(n)}\kappa_0^{(n)}e^{-(u+v_{in})^2}E_1\left\{\sum_n \tau_0^{(n)}(x,x_0)e^{-(u+v_{in})^2}\right\}dx + \right. \\ &\quad \left.\int_{x_0}^{\Delta x}\sum_n \frac{\omega_l^{(n)}}{\omega_u^{(n)}}N_u^{(n)}\kappa_0^{(n)}e^{-(u+v_{in})^2}E_1\left\{\sum_n \tau_0^{(n)}(x_0,x)e^{-(u+v_{in})^2}\right\}dx\right] \qquad (4.17)\end{aligned}$$

and thus

$$\begin{aligned}\Lambda^{(i)}(\tau_0,x_0) = 1- &\frac{1}{2\sqrt{\pi}}\frac{\omega_u^{(i)}}{\omega_l^{(i)}}\frac{N_l^{(i)}(x_0)}{N_u^{(i)}(x_0)}\int_{-\infty}^{\infty}e^{-u^2}\left[\int_0^{x_0}\sum_n\frac{\omega_l^{(n)}}{\omega_u^{(n)}}N_u^{(n)}(x)\kappa_0^{(n)}e^{-(u+v_{in})^2}\times\right. \\ &E_1\left\{\sum_n\tau_0^{(n)}(x,x_0)e^{-(u+v_{in})^2}\right\}dx + \\ &\int_{x_0}^{\Delta x}\sum_n\frac{\omega_l^{(n)}}{\omega_u^{(n)}}N_u^{(n)}(x)\kappa_0^{(n)}e^{-(u+v_{in})^2}\times \\ &\left.E_1\left\{\sum_n\tau_0^{(n)}(x_0,x)e^{-(u+v_{in})^2}\right\}dx\right]du \qquad (4.18)\end{aligned}$$

As in the unblended case, the absorption factor, $\Lambda^{(i)}(\tau_0,x_0)$, depends on the upper level population distribution via the $N_u^{(i)}(x)/N_u^{(i)}(x_0)$ term. In this way the absorption factor is sensitive to the distortion of the upper level population density distribution relative to the optically thin one which places a constraint on the effectiveness of the first order iterative scheme employed here. However, unlike in the emergent flux case ($\bar{g}^{(i)}\{\tau_0\}$), there is also an explicit dependence here upon upper level population densities, $N_u^{(n)}$, in both eqs 4.13 and 4.18. The ratios $N_u^{(n)}/N_u^{(i)}$ are sensitive to opacity and thus further restricts the range of optical depths for which eq. 4.18 may be calculated using the method described in chapter 3. Furthermore, eq. 4.13 must now also be calculated iteratively. However, the purpose of this work is not to develop effective techniques for solving the equations of radiative transfer and statistical balance *simultaneously*, but rather to examine the optical depth regime within which these equations may be *naturally* linearised and de-coupled thus avoiding the need for their simultaneous solution. Eqs 4.13 and 4.18 are calculable using first order techniques

to optical depths beyond the point where the simple escape probability expressions break down. Thus more sophisticated schemes are not necessary here.

Fig. 4.2a shows the C II $2s2p^2\,{}^2D_{5/2}/2s^22p\,{}^2P_{1/2}$ population density ratio versus optical depth, in the blended and unblended cases. These are calculated using eqs 4.13 and 2.39. For this ratio it is clear that the variation with optical depth is more rapid in the blended case than in the unblended case and this is true for all the C II levels. This is not surprising since, as stated above, blending increases the effect of opacity in a line due to absorptions by other lines. Fig. 4.2b shows the C II $2s2p^2\,{}^2D_{3/2}/2s2p^2\,{}^2D_{5/2}$ population density ratio versus τ_0. This curve also demonstrates the dependence of upper level populations upon line blending and illustrates the difficulty in calculating $\bar{\bar{g}}^{(i)}\{\tau_0/2\}$ which depend on such density ratios. These ratios determine the extent to which absorption in a line is influenced by overlapped components and since they depend on both optical depth and linewidth, eq. 4.13 must be calculated iteratively.

In fig. 4.3 $\bar{\bar{g}}^{(i)}\{\tau_0/2\}$ is plotted versus *degree of overlap* (model line width/observed line width) for a selection of spectral lines of C II. This plot corresponds to a single set of optical depths such that the optical depth in the $2s^22p\,{}^2P_{3/2} - 2s2p^2\,{}^2P_{3/2}$ line at 904.143 Å is 3. It is evident from this that blending always leads to a net decreases in the absorption factor – i.e. it increases the effect of opacity upon the population structure. However, it is interesting to note that in the $2s^22p\,{}^2P_{3/2} - 2s^23d\,{}^2D_{3/2}$ line at 687.353 Å, blending initially leads to a decrease in $\bar{\bar{g}}^{(i)}\{\tau_0/2\}$ but this ultimately reverses as the degree of overlap increases. The initial decrease in the absorption factor is due to the increase in absorption of 687.353 Å photons by the $2s^22p\,{}^2P_{3/2} - 2s^23d\,{}^2D_{5/2}$ line at 687.346 Å. The influence of the 687.346 Å component on the 687.353 Å one through blending is determined by the relative strength of the two lines which is determined by the $N_{5/2}/N_{3/2}$ ratio of the C II $2s^23d\,{}^2D$ term. This ratio is also dependent on the degree of blending. The upturn in the $\bar{\bar{g}}^{(i)}\{\tau_0/2\}$ versus degree of overlap trend for the 687.353 Å line corresponds to the increase of emission in the 687.353 Å line due to the enhancement of the $2s^23d\,{}^2D_{5/2}$ level 'winning' over the absorption of photons by the 687.346 Å component.

It can be seen in fig. 4.3 that, as expected, the absorption factor only varies in the cases where there is blending. The indirect effects described above do not influence the

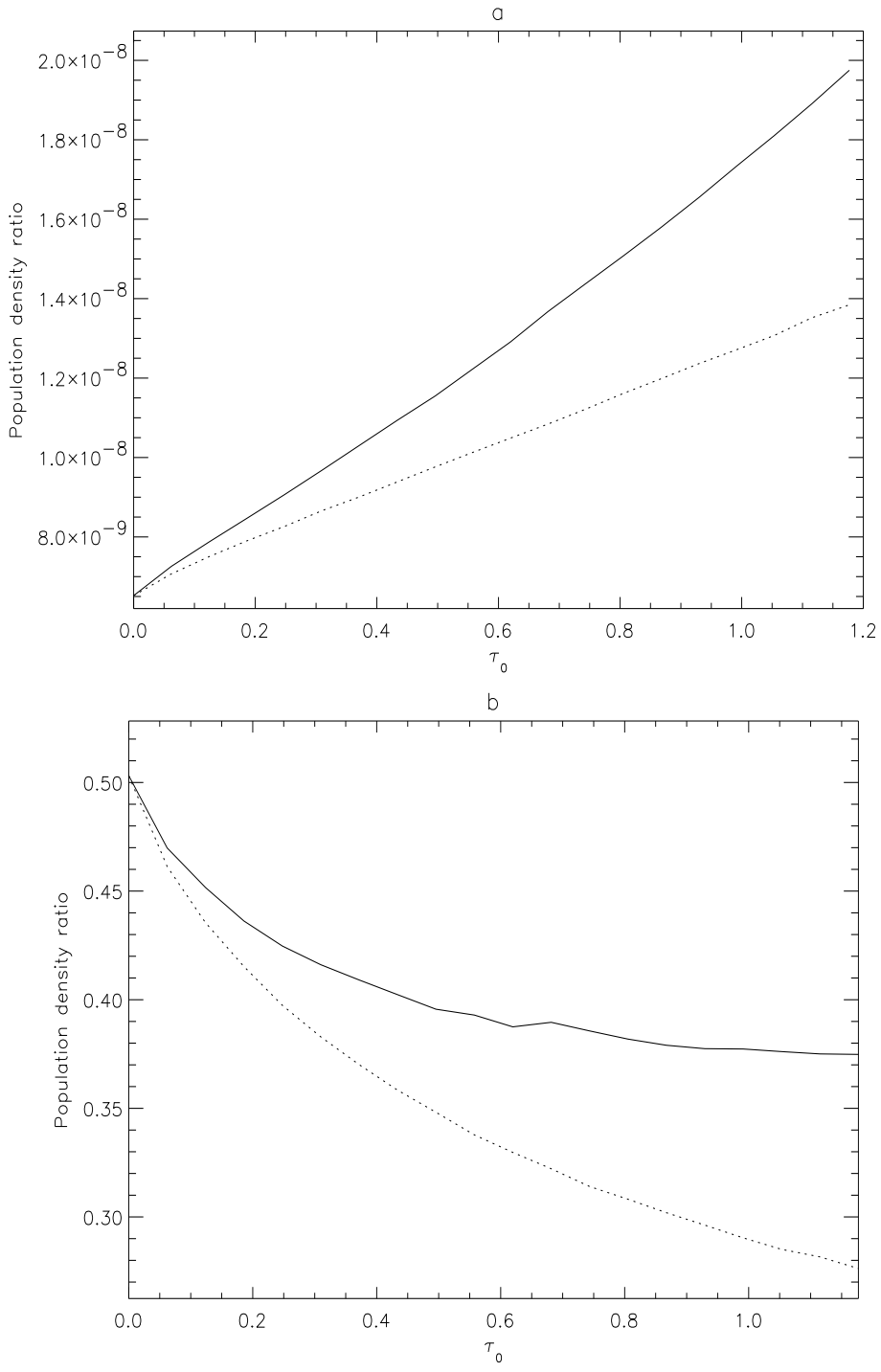

Figure 4.2: Plots of (a) C II $2s2p^2\,{}^2D_{5/2}/2s^22p\,{}^2P_{1/2}$ and (b) C II $2s2p^2\,{}^2D_{3/2}/2s2p^2\,{}^2D_{5/2}$ population density ratios versus τ_0. The solid line corresponds to the blended calculation and the dotted line to the unblended calculation.

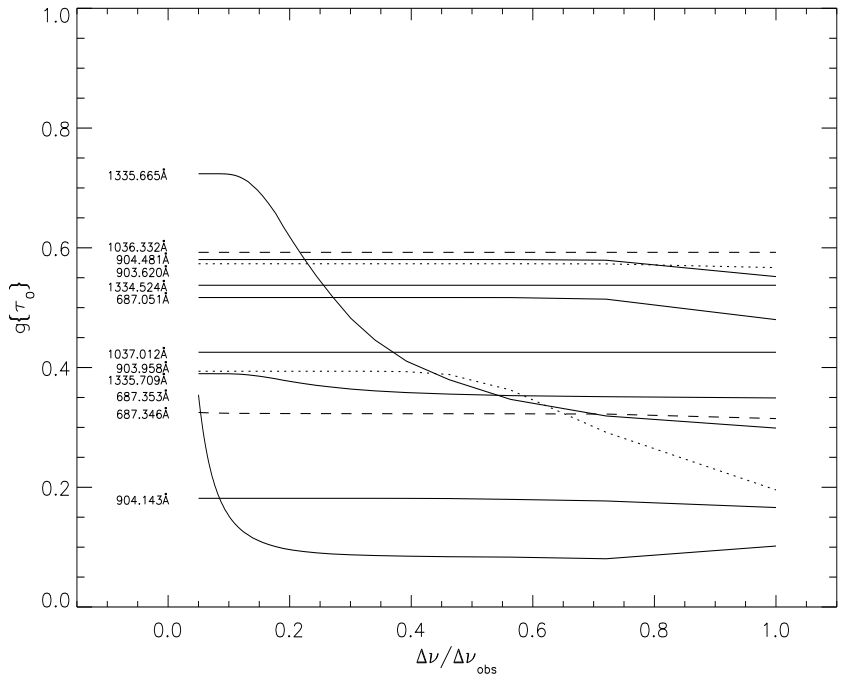

Figure 4.3: $\bar{\bar{g}}^{(i)}\{\tau_0/2\}$ versus *degree of overlap* (model line width/observed line width) for a selection of spectral lines of C II. This plot corresponds to a single set of optical depths such that the optical depth in the $2s^2 2p\,^2P_{3/2} - 2s2p^2\,^2P_{3/2}$ line at 904.143 Å is 3. The variety of line-styles used are to clarify the distinctions between lines.

unblended lines. This is because $\bar{\bar{g}}\{\tau_0/2\}$ (the unblended quantity) is only dependent on optical depth. Consequently the indirect influence of blending on the upper level population densities of *unblended* lines does not manifest itself. Such indirect effects are expected to be present when the spatial dependence of the absorption factor is considered (see sec. 4.4).

4.3 Modelling emergent intensities with blending included

If it is assumed that the source function is constant, or if an optically thick upper level population distribution has been obtained using eq. 4.18, emergent intensities may be calculated in the same way as in sec. 3.9. Blending does not increase the computational complexity of this calculation since neither $g^{(i)}\{\tau_0\}$ nor $\bar{g}^{(i)}\{\tau_0\}$ depend upon upper level population density ratios. Rather they depend on lower level ones which are not sensitive to optical depth.

Fig. 4.4 shows limb brightening curves for the C II $2s^2 2p\,^2P_{3/2} - 2s2p^2\,^2P_{3/2}$ line at 904.143 Å and the C II $2s^2 2p\,^2P_{1/2} - 2s2p^2\,^2P_{3/2}$ line at 903.958 Å. These curves are based on eq. 3.25 in both the unblended and blended cases using $\bar{g}\{\tau_0\}$ (eq. 2.17) and $\bar{g}^{(i)}\{\tau_0\}$ (eq. 4.5) respectively. Though there is still a significant issue of the variation of the source function to address, it is clear that even for a disk centre optical depth of ~ 0.1 blending plays a significant role. Given that the indirect population modification effects seen in chapter 3 influenced the weaker line (the 903.958 Å line) more than the stronger one (the 904.143 Å line), the influence of blending might also be expected to affect the weaker line more. Fig. 4.4b shows, however, that this is not so. Evidently the low optical depth minimises the effect of blending, since the blended and unblended escape probabilities converge as $\tau_0 \to 0$.

A further effect of line blending is to produce an asymmetry in the emergent spectral line profiles. This occurs since overlapped lines are generally displaced in frequency space from one another. The emergent line profiles may be examined from eq. 4.5 since

$$I_\nu \sim \bar{N}_u \frac{1}{\sqrt{\pi}} e^{-u^2} \left[\frac{1 - exp\left\{ -\sum_n \tau_0^{(n)} e^{-(u+v_{in})^2} \right\}}{\sum_n \tau_0^{(n)} e^{-(u+v_{in})^2}} \right] \tag{4.19}$$

If blending is neglected eq. 4.19 is the same as that used by Doyle et al. (2000) to study the effects of line broadening due to opacity in spectral lines from the solar TR. Fig. 4.5a shows the C II $2s^2 2p\,^2P - 2s2p^2\,^2P$ multiplet at ~ 904 Å for a disk centre optical depth of 1, and a line-of-sight optical depth of 10. The calculation uses eq. 4.19

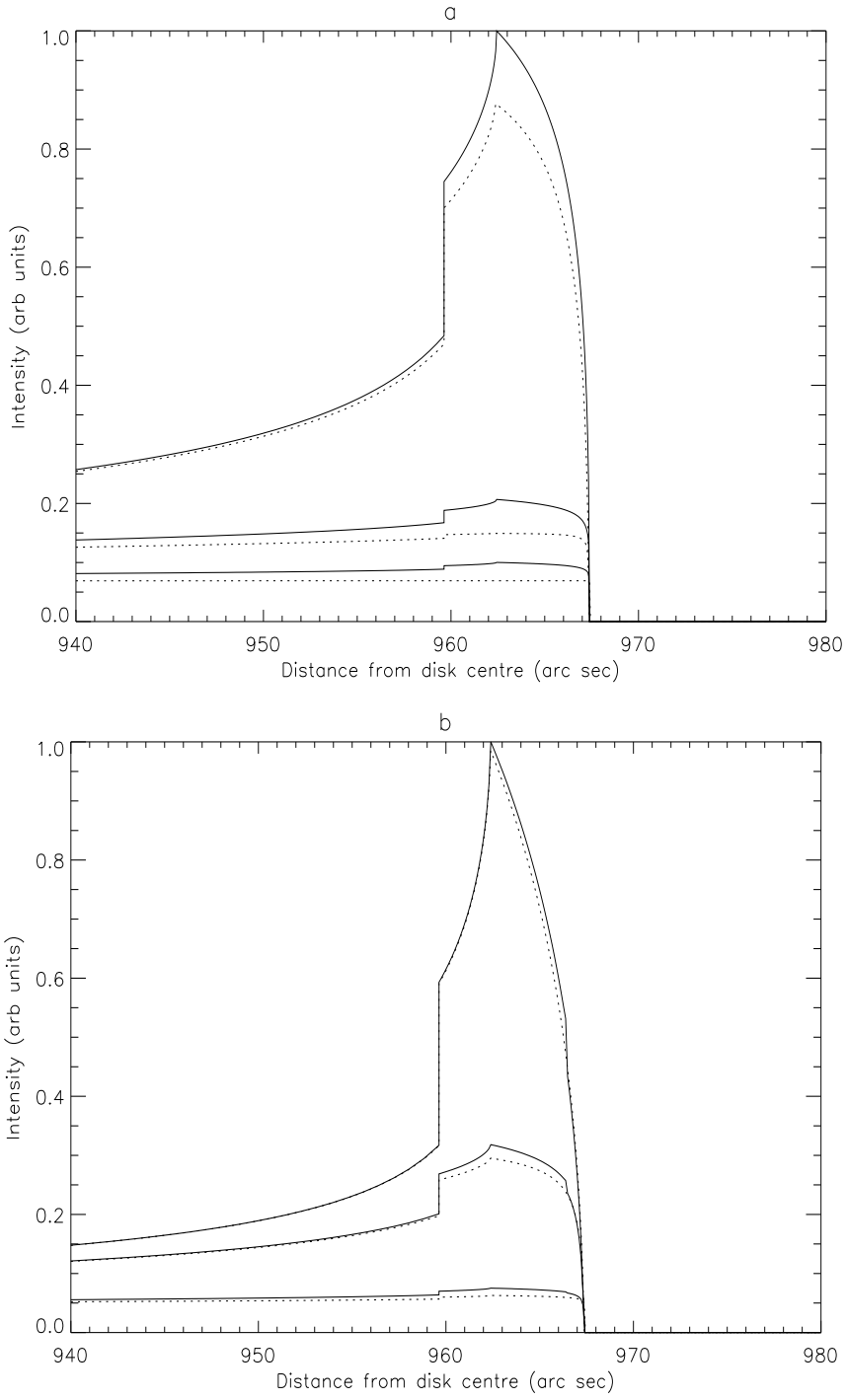

Figure 4.4: Predicted limb-brightening curves for (a) the C II $2s^2 2p^2 P_{3/2} - 2s2p^2\,{}^2P_{3/2}$ line at 904.143 Å and (b) the C II $2s^2 2p^2 P_{1/2} - 2s2p^2\,{}^2P_{3/2}$ line at 903.958 Å, calculated using eq. 3.25 excluding line blending (solid lines) and including line blending (dotted lines). Intensities are calculated in a constant density model. Each graph contains three sets of curves corresponding to disk centre optical depths of 0.1, 1 and 4. The curves are scaled to match at disk centre.

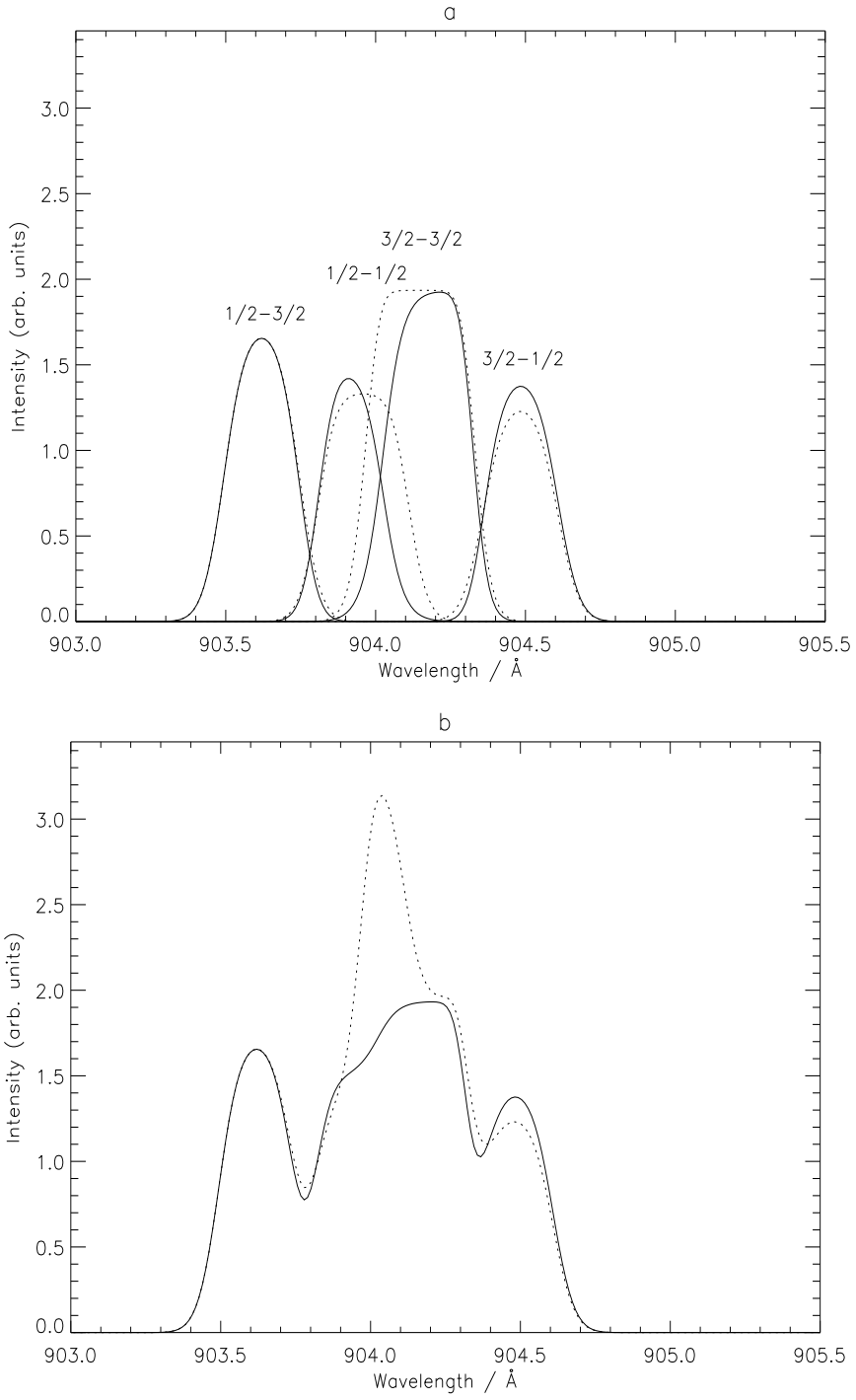

Figure 4.5: (a) Predicted spectral line profiles of the C II $2s^2 2p\,^2P - 2s2p^2\,^2P$ multiplet at ~ 904 Å for a disk centre optical depth of 1, and a line-of-sight optical depth of 10 with blending included (solid line) and blending excluded (dotted line). (b) C II 904 Å multiplet emission summed over each of the lines. Solid and dotted lines as in (a).

and is contrasted with the unblended case. Fig. 4.5b shows the multiplet envelope in each case and illustrates a significant difference to the shape of the multiplet as a whole, especially in the vicinity of the blend. Fig. 4.6 shows in more detail the blended 1/2–1/2 and 3/2–3/2 components. The distortion of the lineshapes is clearly present.

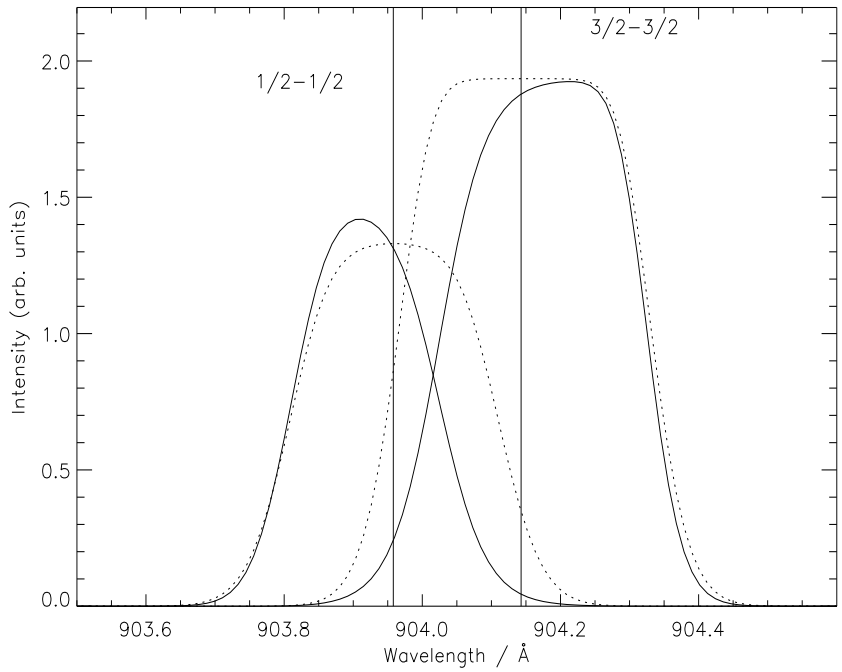

Figure 4.6: Predicted spectral line profiles of the C II $2s^2 2p\,^2P - 2s2p^2\,^2P$ 1/2–1/2 and 3/2–3/2 lines at 903.958 Å and 904.143 Å respectively, with blending included (solid line) and blending excluded (dotted line). The vertical lines indicate the rest wavelengths. Note that blending makes the 1/2–1/2 and 3/2–3/2 components look shifted to the left and right respectively.

Also evident is the further attenuation of the intensity of the 3/2–3/2 component in the blended case as compared with the unblended calculation. This is due to 3/2–3/2 photons being absorbed by the 1/2–1/2 line. In the 1/2–1/2 case, however, the peak intensity is greater when blending is included than when it is not. This seems to be in contradiction to fig. 4.1 which demonstrates that $\bar{g}^{(i)}\{\tau_0\}$ is maximal when there is no blending. That is, the attenuation is minimal in the unblended case. This is true for although the attenuation in the 1/2–1/2 line is increased due to blending with the

3/2–3/2 line, the upper level population density of the $2s2p^2\,{}^2P_{1/2}$ level is enhanced due to absorption of 3/2–3/2 photons in the 1/2–1/2 line. This illustrates the point made at the beginning of the chapter that under certain circumstances blending can lead to an increase in emission. Another interesting feature is that the distortion of the profiles leads to apparent centroid shifts to the blue in the 1/2–1/2 case and to the red in the 3/2–3/2 case.

4.4 The effect of a variable source function on absorption

Shown in figs 4.7 and 4.8 are plots of absorption factors versus position for a selection of spectral lines of C II and for three sets of optical depths. These figures are similar to figs 3.5 and 3.6 but with line blending included. A further difference is that the sets of optical depths correspond to values in the control line (the $2s^22p\,{}^2P_{3/2} - 2s2p^2\,{}^2P_{3/2}$ line at 904.143 Å as before) of 0.1, 1 and 4 as opposed to 0.1, 1, and 10 in the figures of chapter 3. As in figs 3.5 and 3.6 the absorption factor calculations are computed within a constant density atmosphere model. The main features of these graphs may be summarised as follows:

The 1335 Å multiplet

The $2s^22p\,{}^2P_{3/2} - 2s2p^2\,{}^2D_{5/2}$ line at 1335.709 Å shows a slight deviation due to blending with the $2s^22p\,{}^2P_{3/2} - 2s2p^2\,{}^2D_{3/2}$ line at 1335.665 Å which is more optically thin. The 1335.665 Å line itself displays a significant deviation due to blending with the 1335.709 Å component. The 1335.665 Å line is also indirectly modified due to the $2s^22p\,{}^2P_{1/2} - 2s2p^2\,{}^2D_{3/2}$ line at 1334.524 Å (see sec. 3.5). The 1334.524 Å line is as before (sec. 3.5) with a slight modification due to indirect effects caused by the line at 1335.665 Å.

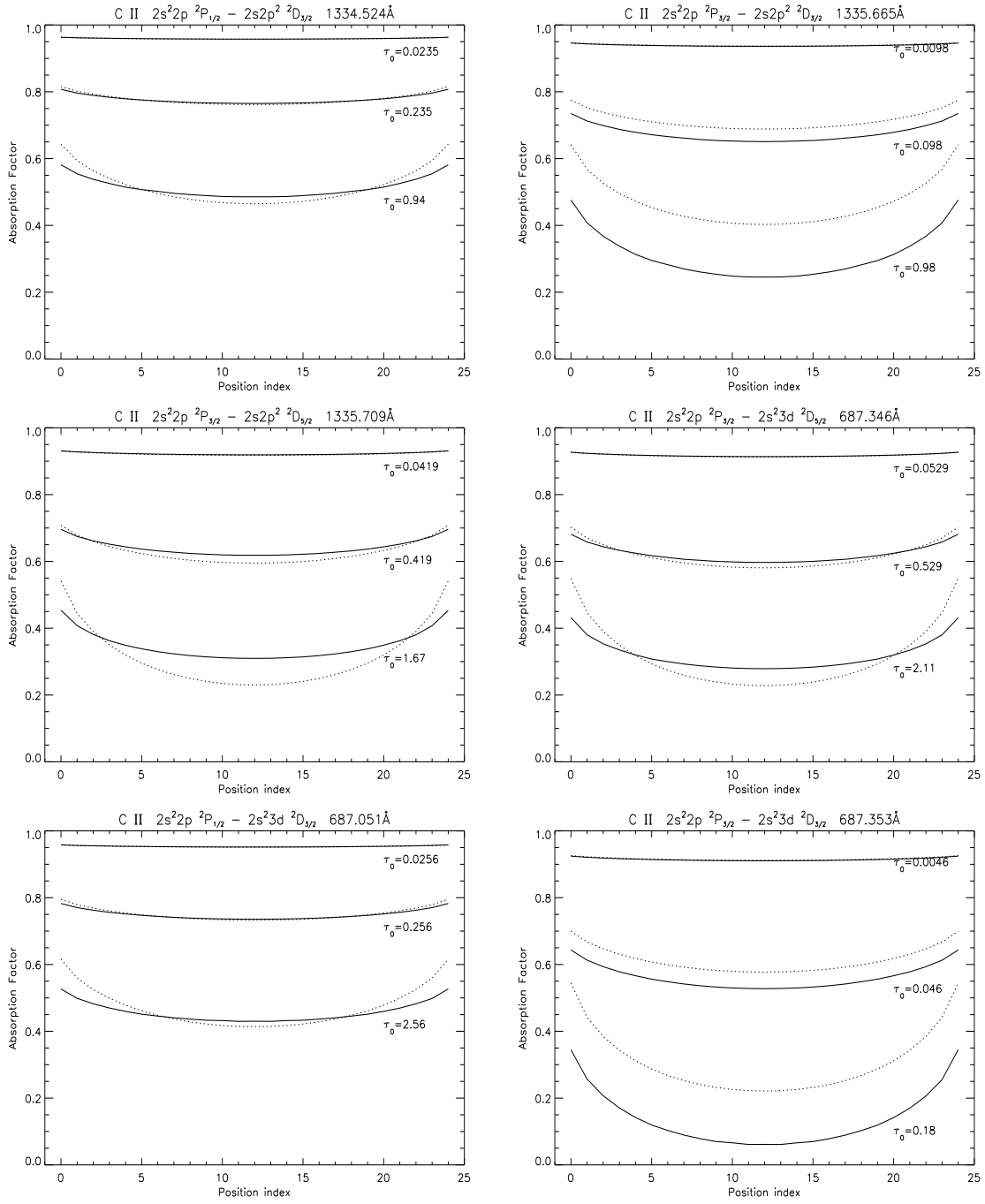

Figure 4.7: Absorption factors with blending included versus position for selected lines of C II corresponding to three sets of optical depths. Absorption factors are calculated iteratively via eqs 4.18 and 2.8. The solid lines are $\Lambda^{(i)}(\tau_0, x)$ and the dotted lines are $\mathcal{G}^{(i)}\{\tau_0, x\}$.

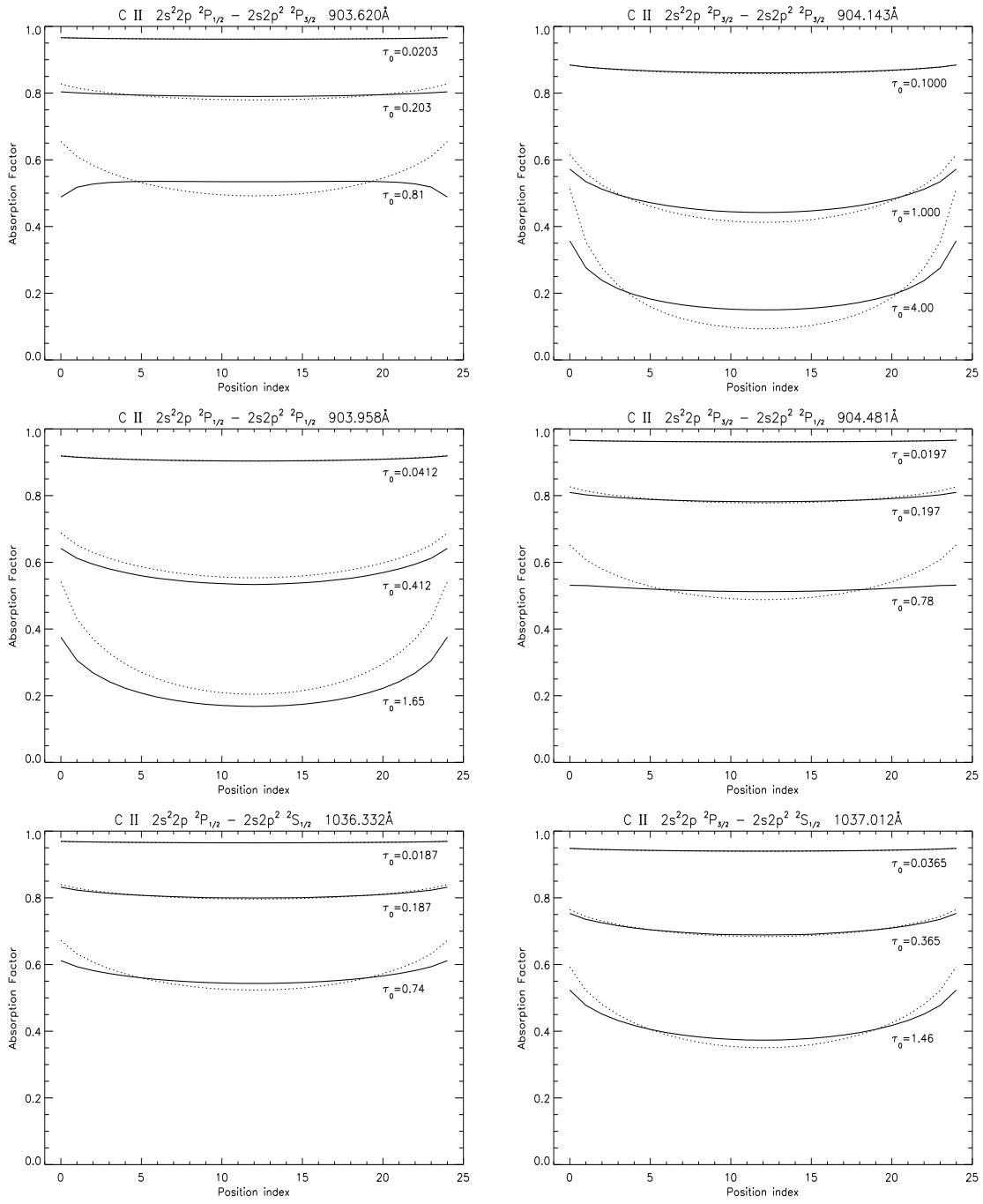

Figure 4.8: Absorption factors with blending included versus position for selected lines of C II as in fig 4.7.

The 687 Å multiplet

The $2s^2 2p\,^2P_{3/2} - 2s^2 3d\,^2D_{5/2}$ line at 687.346 Å shows a slight deviation due to blending with the $2s^2 2p\,^2P_{3/2} - 2s^2 3d\,^2D_{3/2}$ line at 687.353 Å. The $2s^2 2p\,^2P_{1/2} - 2s^2 3d\,^2D_{3/2}$ line at 687.051 Å shows minor modification due to blending with the 687.346 Å line and also moderate modification from indirect effects again due to the 687.346 Å component. The line at 687.353 Å displays significant deviation due to blending with the 687.346 Å component which is more optically thick. There is also indirect modification due to the 687.051 Å line.

The 904 Å multiplet

The $2s^2 2p\,^2P_{1/2} - 2s2p^2\,^2P_{3/2}$ line at 903.620 Å is, as before (see sec. 3.5), indirectly modified due to the $2s^2 2p\,^2P_{3/2} - 2s2p^2\,^2P_{3/2}$ line at 904.143 Å. The 904.143 Å line shows slight modification due to blending with the $2s^2 2p\,^2P_{3/2} - 2s2p^2\,^2P_{1/2}$ and $2s^2 2p\,^2P_{3/2} - 2s2p^2\,^2P_{1/2}$ lines at 903.958 Å and 904.481 Å respectively. The 904.481 Å component displays slight deviation due to blending with the 904.143 Å line and there is indirect modification due to the 903.958 Å component.

The 1036 Å multiplet

These lines are not blended together and they do not share upper levels with any of the above lines. Thus their absorption factors are as before (see sec. 3.5).

Discussion

As in the unblended case, the source function variation manifests itself in eq. 4.18 via the $N_u(x)/N_u(x_0)$ term. Thus it is the shape of the $N_u(x)$ versus x curve that comes into play and not the absolute value of $N_u(x)$. Blending, however, introduces a dependence of the integrand of this equation on $N_u^{(i)}(x)/N_u^{(j)}(x)$ where i and j indicate separate lines in a blend. The effect of this is to decrease the absorption factors everywhere as compared with $\mathcal{G}^{(i)}(\tau_0, x)$. This decrease acts to shift the absorption factor curves downward rather than to distort them further. It is not sufficient,

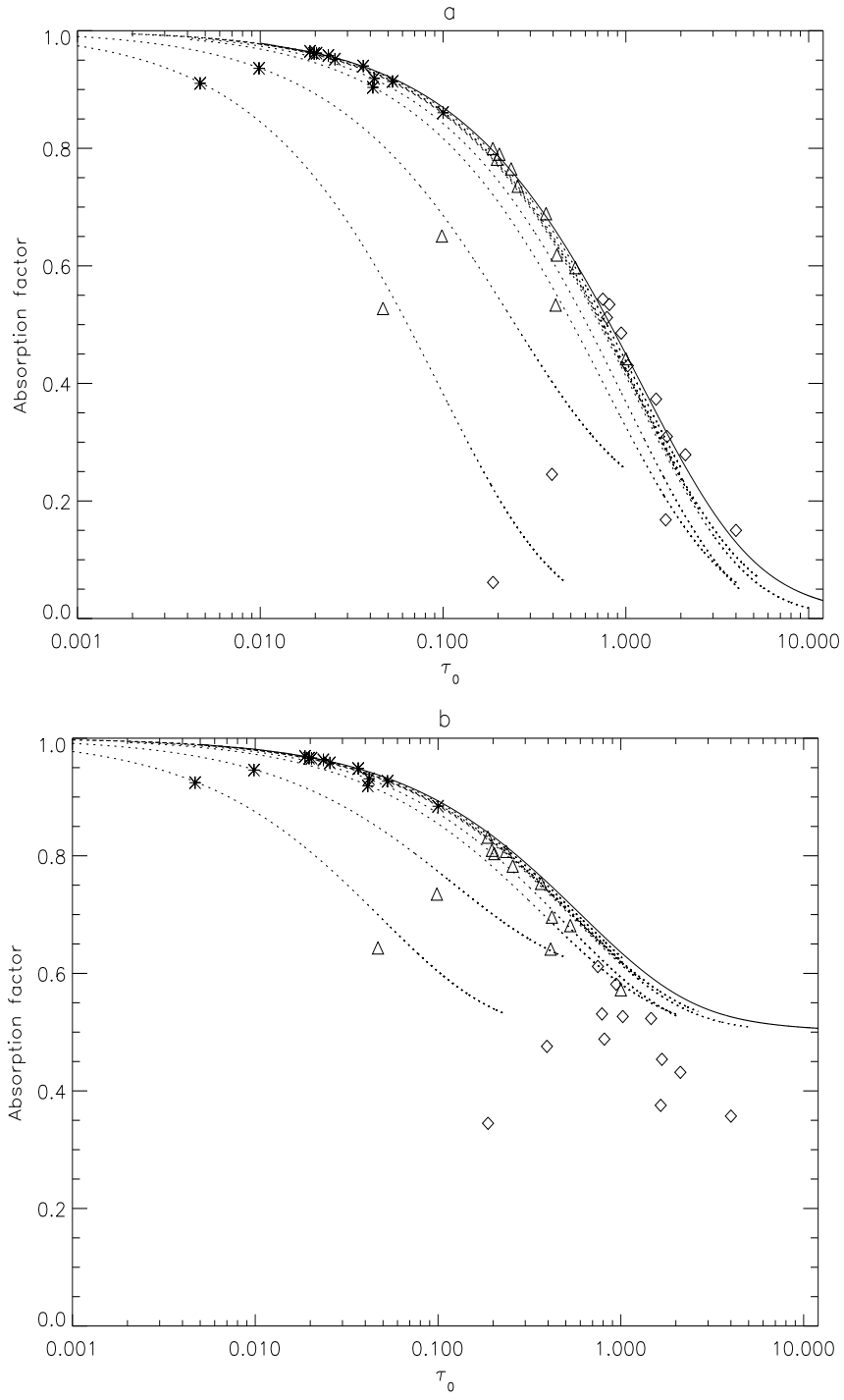

Figure 4.9: Absorption factors including line blending at (a) layer centre ($x = D/2$) and (b) layer edge ($x = 0$) versus optical depth for the constant lower level density model, taken from the plots in figs 4.7 and 4.8. The *'s, $\triangle$'s and $\diamond$'s are the absorption factors, $\Lambda^{(i)}(\tau_0, x)$ (eq. 4.18), corresponding to the three sets of optical depths. The solid line is $\mathcal{G}(\tau_0, x)$ and the dotted lines are $\mathcal{G}^{(i)}(\tau_0, x)$.

however, to say that blending effectively increases the optical depth, although this is certainly an effect (see the summation of optical depths in eq. 4.18).

It is clear that the effects of blending are more severe than the indirect effects on thin lines with thick partners, discussed in chapter 3. Furthermore, blending is more apt to affect lines that markedly influence the population distribution – i.e. the stronger (thicker) lines – unlike the indirect effects which mainly alter the absorption factors of the weaker (thinner) lines.

4.5 The validity of $\mathcal{G}^{(i)}(\tau_0, x)$ in the blended case

It is clear from figs 4.7 and 4.8 that blending decreases the range of optical depths for which $\mathcal{G}(\tau_0, x)$ is effective for describing self absorption in spectral lines. Previously the absorption factors of the strongest and most dominant lines – that is, those that most significantly influence the population structure calculation – broadly speaking followed the $\mathcal{G}(\tau_0, x)$ versus x trend. Moreover, they were in fairly close agreement at layer centre (see figs 3.5 and 3.6). With blending included, though the trends still follow those of $\mathcal{G}^{(i)}(\tau_0, x)$ (indirectly modified lines excepting), the layer centre values can be markedly different (see, for example, the $2s^2 2p\,^2P_{3/2} - 2s2p^2\,^2D_{3/2}$ line at 1335.665 Å shown in fig. 4.7). Significantly, it is not just the weaker, less important (with respect to the population calculation) lines that are so affected.

Figs 4.9a and b show the blended absorption factors at layer centre (a) and the layer edge (b). Unlike the unblended case (see fig. 3.7), at layer centre the absorption factor can not be considered a monotonic decreasing function of optical depth since it is line specific. As in the unblended case, at layer centre $\mathcal{G}^{(i)}(\tau_0, D/2)$ is effective for moderate optical depths. However, for significantly blended lines the optical depth regime where this is true is reduced as compared with the unblended case. At the layer edge indirect effects come into play and $\mathcal{G}^{(i)}(\tau_0, 0)$ (which is identical to $\mathcal{G}^{(i)}(\tau_0, D)$ in the constant density case) is less effective.

Fig. 4.9a displays a degree of agreement between $\mathcal{G}^{(i)}(\tau_0, D/2)$ (i.e. $\bar{\bar{g}}^{(i)}\{\tau_0/2\}$) and $\Lambda^{(i)}(\tau_0, D/2)$ that is greater than that implied by figs 4.7 and 4.8. In the latter two figures the $\mathcal{G}^{(i)}(\tau_0, x)$ values are calculated without iteration. That is, they represent

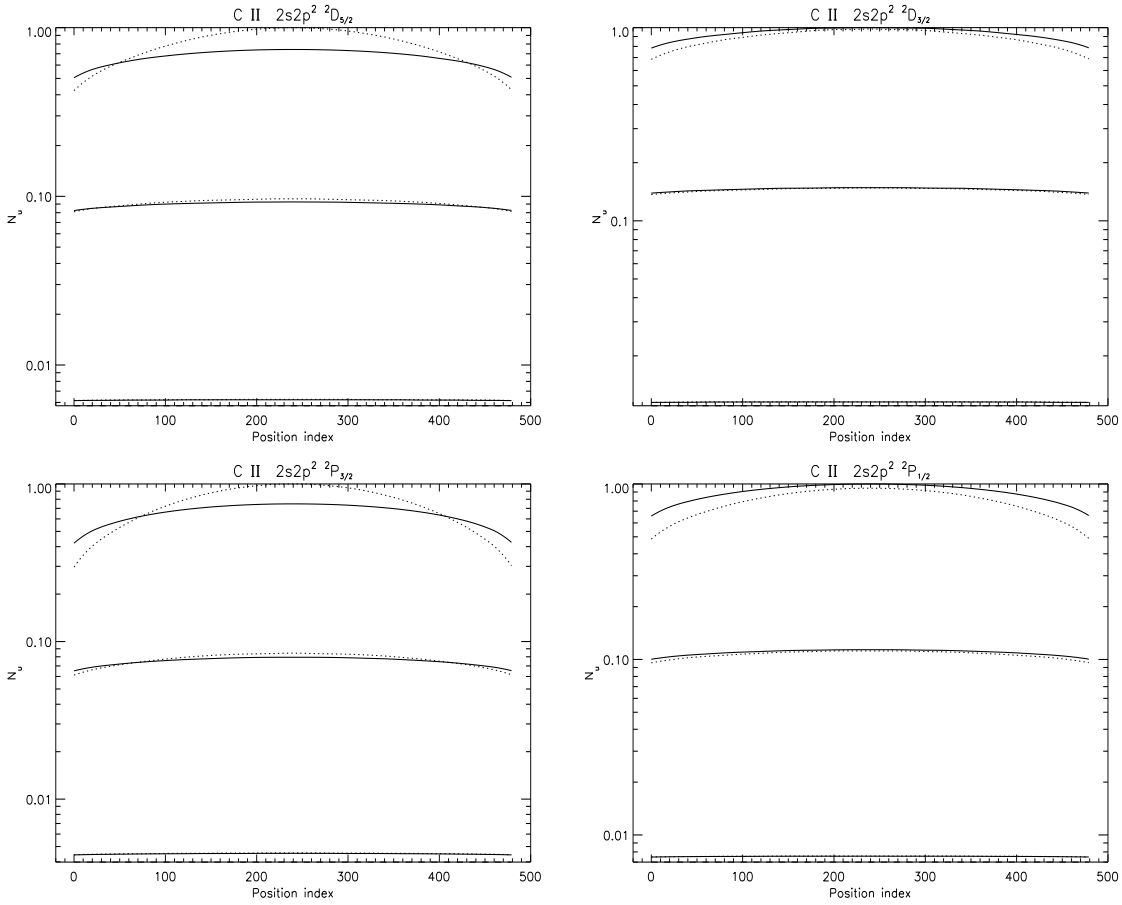

Figure 4.10: Upper level population densities versus spatial position for selected lines of C II. The solid lines correspond to calculations based on $\Lambda^{(i)}(\tau_0, x)$ for the same three sets of optical depths as in figs 4.7 and 4.8. The dotted lines represent the $\mathcal{G}^{(i)}(\tau_0, x)$ based calculations. Values are not absolute but are scaled so that the maximum population density value is unity.

the initial values of the absorption factor in the iterative process. In general, however, $\mathcal{G}^{(i)}(\tau_0, x)$ must be computed iteratively due to its explicit dependence on upper level population density ratios of overlapped lines. In figs 4.9a and b the $\mathcal{G}^{(i)}(\tau_0, x)$ values are computed iteratively and are thus closer to the $\Lambda^{(i)}(\tau_0, x)$ values. Figs 4.9a and b are therefore indicative of the influence of the modification of the source function due to opacity upon absorption factors in the case where blending is included.

The usefulness of the escape probability techniques is that they represent accurate solutions to the radiative transfer and statistical balance equations in a regime in which these equations naturally linearise and de-couple. Line blending re-introduces

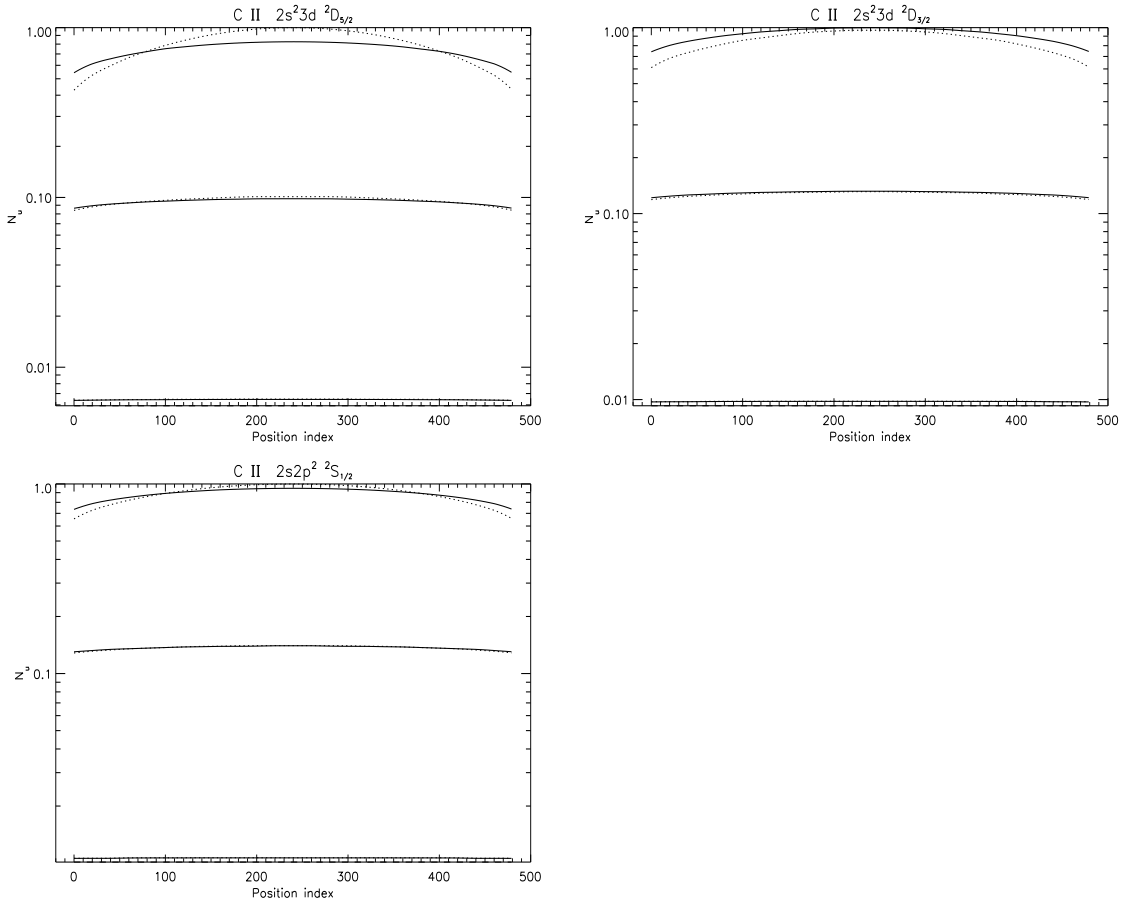

Figure 4.11: Upper level population densities versus spatial position for selected lines of C II. The solid and dotted lines are as in fig. 4.10.

non-linearity into the statistical balance equations via the dependence of the absorption factor on upper level population density ratios. To perform an iterative process to calculate $\mathcal{G}^{(i)}(\tau_0, x)$ therefore compromises the appeal of the absorption factor approach. Computational simplicity may be restored, however, by simply ignoring this non-linearity and utilising upper level population densities deduced from an optically thin calculation thus further restricting the optical depth regime within which $\mathcal{G}^{(i)}(\tau_0, x)$ is effective. In this respect figs 4.7 and 4.8 demonstrate the applicability, or otherwise, of $\mathcal{G}^{(i)}(\tau_0, x)$ for practical use. In these figures the $\Lambda^{(i)}(\tau_0, x)$ curves often seem to follow the $\mathcal{G}^{(i)}(\tau_0, x)$ trends but are shifted downward. If $\mathcal{G}^{(i)}(\tau_0, x)$ is

calculated iteratively then these downward shifts disappear and the results are similar to those of chapter 3, with the deviation of $\Lambda^{(i)}(\tau_0, x)$ from $\mathcal{G}^{(i)}(\tau_0, x)$ minimal at layer centre and significant at the edge, characterised by the degree of distortion of the upper level with respect to the lower. However, the fact that blending effectively increases the optical depth serves to restrict the region of validity of the $\mathcal{G}^{(i)}(\tau_0, x)$ quantity. Nevertheless a spectral line classification that includes the effects of line blending is possible using $\bar{\bar{g}}^{(i)}\{\tau_0/2\}$ providing an iteration process is performed. The validity of this classification is optical depth and line dependent. For most of the C II lines $\bar{\bar{g}}^{(i)}\{\tau_0/2\}$ is effective, as in the unblended case, for disk centre optical depths up to ~ 1. For the most severely blended lines, however, the restriction is more severe.

4.6 The effect of blending upon the density distributions

Upper level population densities for the C II lines in figs 4.7 and 4.8 for the same three sets of optical depths are shown in figs 4.10 and 4.11. These plots have a logarithmic scale that masks somewhat the true extent of the distortion of upper levels. Plots of the same for just the maximum optical depths are shown on a linear scale in figs 4.12 and 4.13.

Increased absorption in blended lines distorts the upper level population density distributions with respect to the lower ones in a manner that increases with optical depth. This effect was seen in the unblended case (see sec. 3.7) but is more severe here since blending serves to increase the radiation field in an overlapped line and also increases the effective optical depth. Moreover, the dependence upon upper level density ratios, discussed in sec. 4.4, has a marked effect upon the absorption factors but does not significantly alter the *shape* of the upper level population density distortion. That is, this secondary effect of blending leads to a population modification which is approximately constant in space. This is significant since it is the extent of the distortion rather than the absolute value of the modification that determines

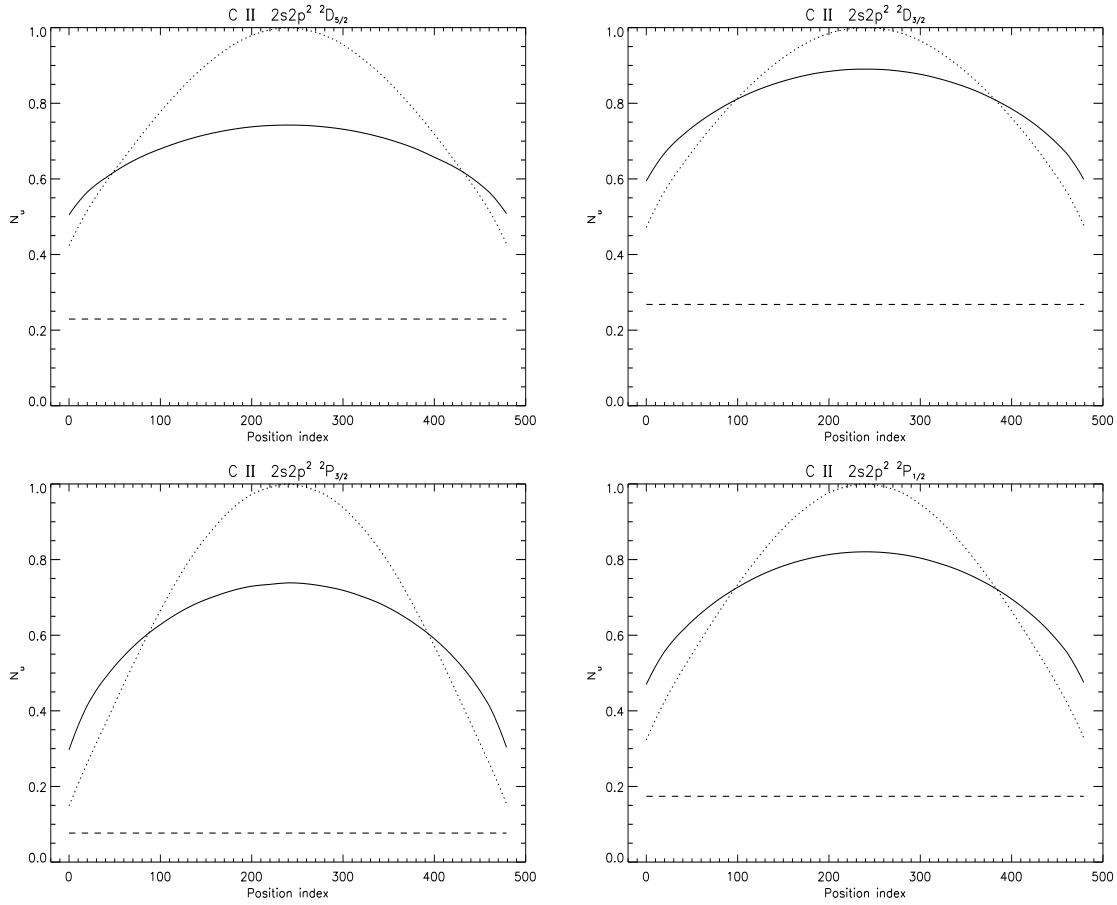

Figure 4.12: Upper level population densities versus spatial position including blending effects, for selected lines of C II as in figs 4.10 and 4.11 but just in the most optically thick case. The solid and dotted lines are as in figs 4.10 and 4.11. Values are not absolute but are scaled so that the maximum population density value is unity.

the validity, or otherwise, of the line-of-sight averaged escape probability. The absolute value of the absorption factor is dependent upon these ratios, hence the need to calculate $\mathcal{G}^{(i)}(\tau_0, x)$ iteratively. However, line blending only influences the validity of the line-of-sight averaged escape probability through the increase in effective optical depth.

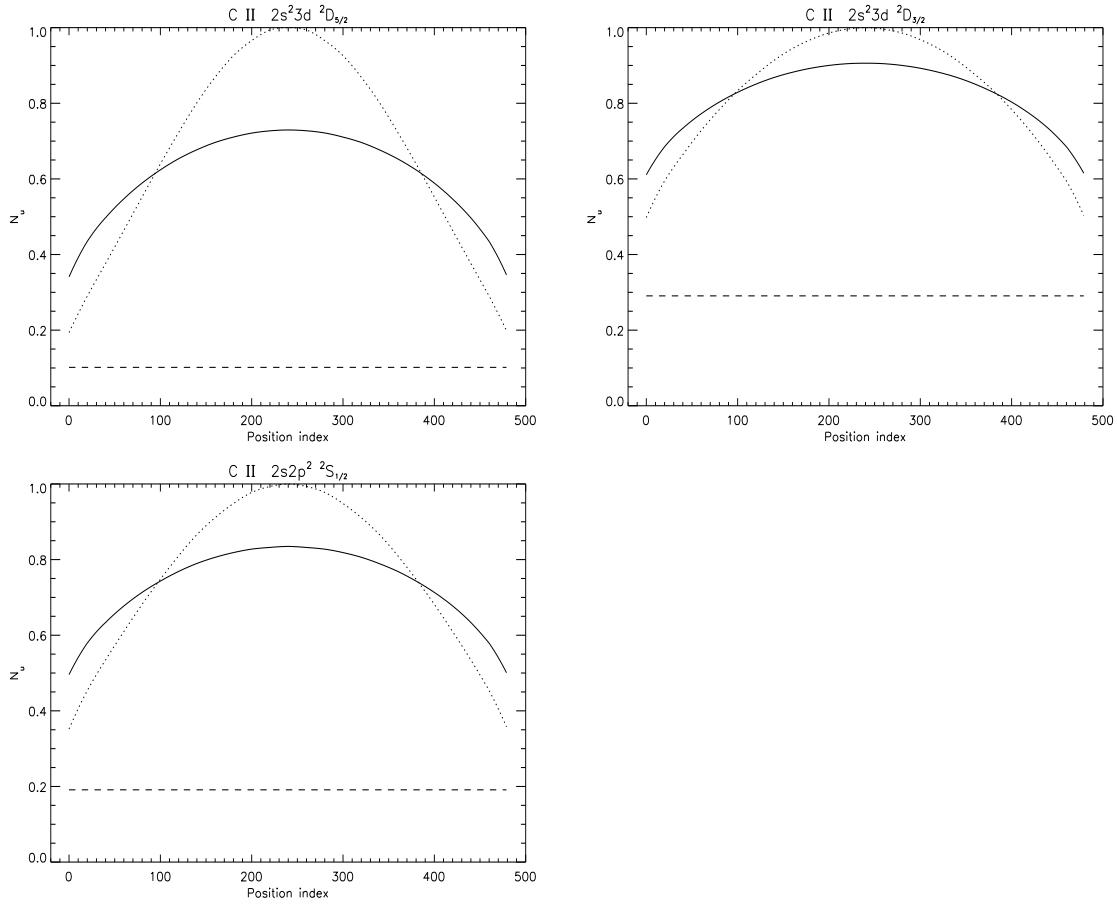

Figure 4.13: Upper level population densities versus spatial position including blending effects, for selected lines of C II as in fig. 4.12.

4.7 The effect of line blending on emergent fluxes

Figs 4.14a and b show predicted limb-brightening curves for the C II $2s^2 2p\,^2P_{3/2} - 2s2p^2\,^2P_{3/2}$ line at 904.143 Å, contrasting the *resolved* (population modification included) calculation with the *unresolved* (no population modification included) calculation. Line blending is included in both figures via eqs 4.4 and 4.5 respectively. These figures illustrate that for optical depths up to ~ 4 the modification to the population density distribution due to opacity, impinges minimally upon the limb-brightening curves. That is, it is sufficient to assume that the only effect of opacity is to scatter photons out of the line-of-sight, even when line blending is included, for

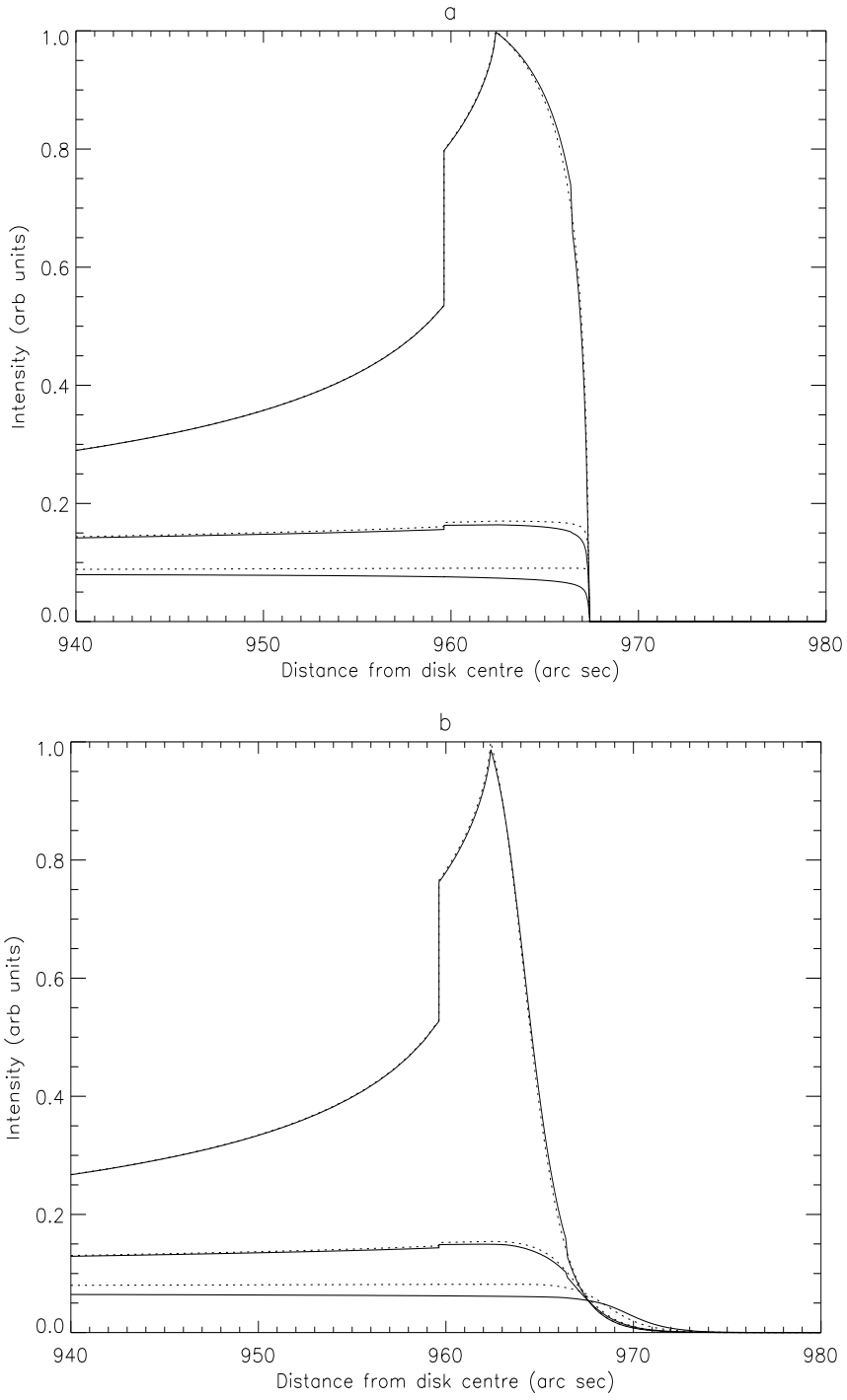

Figure 4.14: Predicted limb-brightening curves for the C II $2s^2 2p\,^2P_{3/2} - 2s2p^2\,^2P_{3/2}$ line at 904.143 Å. The solid lines correspond to calculations including line blending and the modification to the upper level population density distribution due to opacity using $g^{(i)}\{\tau_0\}$ and $\Lambda^{(i)}(\tau_0, x)$ (eqs 4.4 and 4.18 respectively). The dotted lines correspond to calculations including line blending and assuming constant source function using $\bar{g}^{(i)}\{\tau_0\}$ (eq. 4.5). Intensities are calculated in (a) a constant density model and (b) a model with density that decreases exponentially with height. Each plot contains three sets of curves corresponding to disk centre optical depths of 0.1, 1 and 4. The curves are scaled to match at disk centre.

optical depths in this range.

Figs 4.15a and b show the same as 4.14a and b but here the blended, resolved calculation is contrasted with the unresolved, unblended one. It is clear from these figures that blending has a more significant impact on the limb-brightening curves than the population modification.

4.8 Concluding remarks

From an algebraic perspective, the effects of spectral line blending may be incorporated easily within the escape probability and absorption factor expressions. However, blending re-introduces non-linearity into the optically thick statistical balance equation thus compromising the simplicity of the absorption factor approach. Blending leads to photons that are emitted in one line being absorbed by another which in turn leads to a sensitivity of the absorption factor to the ratio of upper level population densities of overlapped components. These ratios are themselves opacity sensitive. Consequently blending markedly influences the absorption factors. It does so in two ways. The first is due to the increase in effective optical depth which may in principle be characterised by an unblended calculation with a modified optical depth. This effective optical depth is always larger than the unblended one. The second way is due to the dependence of the absorption factor on upper level population density ratios and leads in general to a decrease in the absorption factor. It is, however, largely independent of spatial position and so does not further distort the resultant upper level population density distributions and therefore does not impinge on the validity of the line-of-sight averaged escape probability.

The validity of $\mathcal{G}^{(i)}(\tau_0, x)$ follows as in chapter 3, and is dominated by the indirect effects evident in lines that share an upper level with a more optically thick line. However, this is only true if $\mathcal{G}^{(i)}(\tau_0, x)$ is calculated iteratively. If iteration is not performed then $\mathcal{G}^{(i)}(\tau_0, x)$ is ineffective for blended lines even for small optical depths.

As in chapter 3, the $\bar{g}^{(i)}\{\tau_0\}$ quantity (eq. 4.5) is effective for optical depths up to some maximum. With blending included this cut-off is reduced from ~ 10 to ~ 4. It is clear from fig. 4.15 that the error introduced by the neglect of the modification to

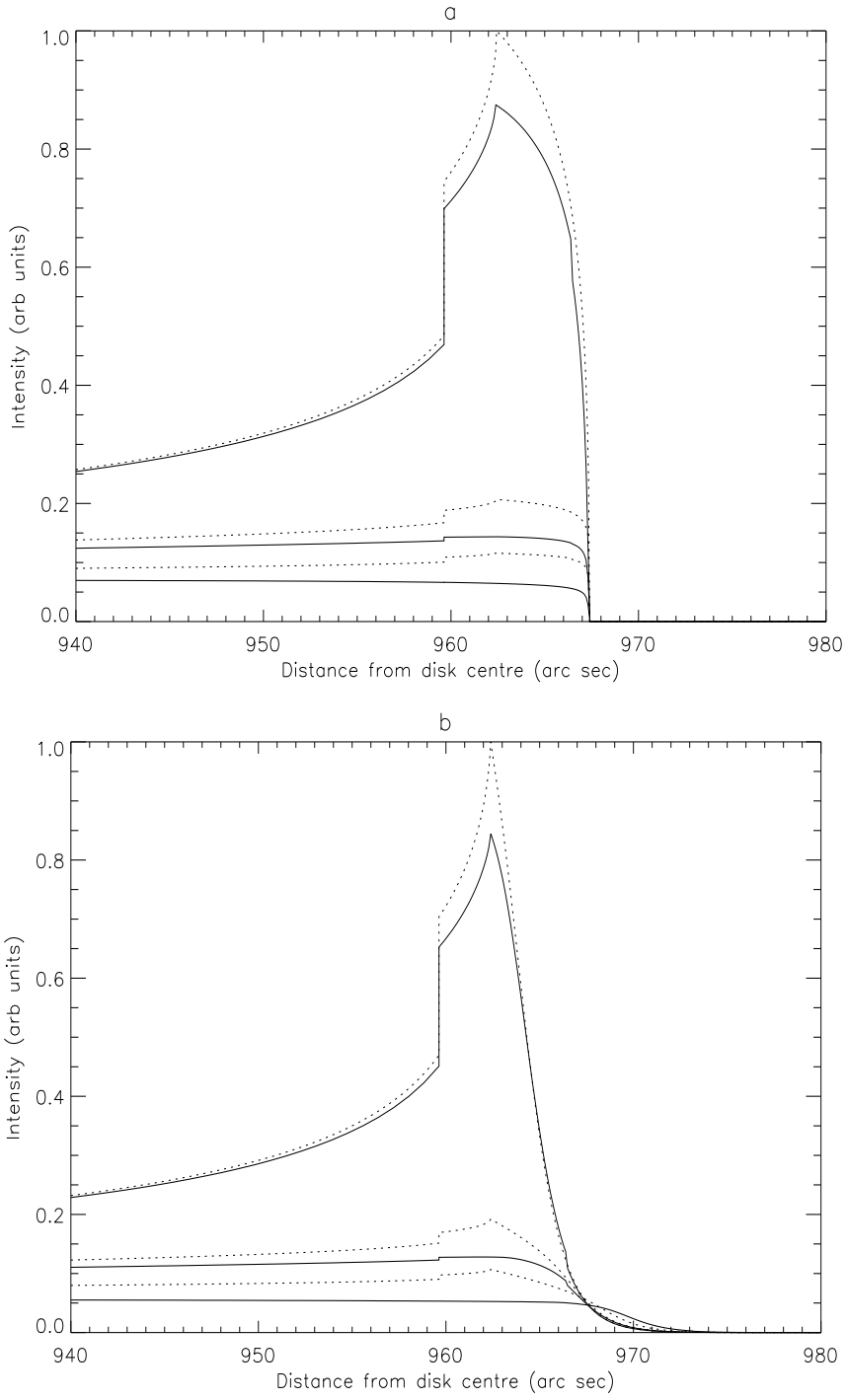

Figure 4.15: Predicted limb-brightening curves for the C II $2s^2 2p\,^2P_{3/2} - 2s2p^2\,^2P_{3/2}$ line at 904.143 Å as in fig. 4.14. The solid lines correspond to calculations including line blending and the modification to the upper level population density distribution due to opacity. The dotted lines correspond to calculations neglecting both line blending and the modification to the upper level population density distribution.

the source function due to opacity is negligible compared to that due to the neglect of line blending. Even at an optical depth of 0.1 blending significantly modifies the emergent fluxes. Thus a regime exists where opacity effects are significant and $\bar{g}^{(i)}\{\tau_0\}$ is effective. Moreover, both the C II and C III datasets discussed in chapter 2 fall within this regime.